PFC/RR-86-16

DOE/ET-51013-187
UC20g

RUNAWAY ELECTRON DISTRIBUTIONS AND THEIR STABILITY WITH RESPECT TO THE ANOMALOUS DOPPLER RESONANCE

V. Fuchs,* M. Shoucri,*
J. Teichmann,** and A. Bers

June 1986

Plasma Fusion Center
Massachusetts Institute of Technology
Cambridge, Massachusetts 02139 USA

* IREQ, Varennes, Quebec, Canada JOL 2PO.

**University of Montreal, Montreal, Quebec, Canada HC 3J7.

This work was supported in part by Hydro-Quebec Project No. 01584-57358713, in part by DOE Contract No. DE-ACOL-78ET-51013, and in part by NSF Grant ECS 85-15032.

RUNAWAY ELECTRON DISTRIBUTIONS AND THEIR STABILITY WITH RESPECT TO THE ANOMALOUS DOPPLER RESONANCE

V. Fuchs, M. Shoucri and J. Teichmann[a)]

Tokamak de Varennes, IREQ, Varennes, Québec, Canada, J0L 2P0

A. Bers

Plasma Fusion Center, Massachusetts Institute of Technology,

Massachusetts, U.S.A., 02139

The stability of non-relativistic runaway electron distributions with respect to the anomalous Doppler resonance is examined in a range of parameters of interest to Tokamaks, i.e. for $Y \equiv \omega_{pe}/\Omega_{ce} \leq 2$ and for ohmic electric fields $\varepsilon \equiv E/E_c \leq 0.1$. Distribution functions are calculated numerically within a region up to 35 v_e (thermal velocities) using a finite-element 2-D Fokker-Planck code. Alternatively, an analytic approximation for the runaway distribution function is used, valid beyond the critical velocity $v_c \simeq v_e\,(E_c/E)^{\frac{1}{2}}$. Stability thresholds in $(\omega, k_\parallel)$ - space are then determined. For example, for $Y = 1$ and $\varepsilon = 0.1$, and providing that the runaway tail extends at least to 30 v_e, unstable waves exist having $\omega \lesssim 0.6\ \Omega_{ce}$ and $k_\parallel \lesssim 0.03\ \Omega_{ce}/v_e$.

a) Permanent address: Département de Physique, Université de Montréal, Montreal, Quebec, Canada, H3C 3J7.

I. INTRODUCTION

The response of a plasma to an applied steady electric field E is one of the central problems in Tokamak physics and has been during the past two decades the subject of interest of a number of theoretical studies.[1-6] Some of the theory, but mainly the experimental effort in this field has been recently reviewed by Knoepfel and Spong.[7] The basic effect resulting from the application of a steady electric field to a distribution of electrons is the generation of runaway electrons forming a raised suprathermal "runaway" tail in the direction opposite to the applied electric field. Since under certain conditions runaway electrons can cause damage to the confining structures, it has been of great importance to determine their distribution function and more particularly the runaway production rate associated with them.[2-6] Since these distributions possess a typically high degree of temperature anisotropy, an important problem which also has received some attention[8-12] is the linear stability of magnetized plasma waves. Roughly speaking, instability occurs when Landau damping (given by $\partial f/\partial v_\parallel$ at $v_\parallel = v_L = \omega/k_\parallel$) cannot compensate for the destabilizing effect of the anomalous Doppler resonance [given by the value of f at $v_\parallel = v_{AD} = (\omega + \Omega_{ce})/k_\parallel$].

In this work we use a finite-element boundary-value code and semi-analytic techniques to investigate runaway distributions and their stability with respect to the anomalous Doppler resonance. We limit our attention to the investigation of conditions for the onset of the instability, and we therefore do not include in the formalism the effect of wave-induced pitch-angle

scattering of electrons. We report here that our results are in agreement with those of Wiley et al.[12], but in disagreement with Refs. 9, 10 and 11.

The present work was motivated to some extent by the disparity we find in the literature[9-12] as regards the predicted parameter space for the runaway instability. The disagreement on the calculated values of the growth rate can be traced to uncertainty in the evaluation of Landau damping, this resonance being situated at $v_L = \omega/k_\parallel$ which is nearer to the bulk of the distribution than is the anomalous Doppler resonance v_{AD}. Hence v_L is situated in a region where f varies relatively rapidly, and where uncareful modeling of the distribution function can seriously misrepresent the actual value of $\partial f/\partial v_\parallel$. In contrast, the anomalous Doppler resonance (ADR) is located in a region of high temperature anisotropy, i.e. far out on the runaway tail at a position $v_{AD} > 2\ v_L$. There, the tail is relatively flat and its height directly proportional to the induced particle flow, i.e. to the runaway rate which is a known function[3,5,6,13] of ion charge Z_i and electric field E. Since the effect of the ADR is essentially determined by the number of electrons supporting the wave, its contribution to the growth rate can be therefore estimated in a straightforward manner.

Amongst the quoted stability studies[9-12], most accurate appear to us the results of Wiley et al.[12], based upon a distribution function f obtained numerically within the range $v \leq 20\ v_e$ ($v_e^2 = kT_e/m_e$) from a 2-D Fokker-Planck code. Beyond that range they extrapolate f in the form

$$f \simeq \frac{F\ (v_\parallel)}{2\pi\ T_\perp\ (v_\parallel)} \exp\ (-v_\perp^2/2T_\perp), \tag{1}$$

$$F = a + b/v_\parallel^3,\ T_\perp = c + d\ \ln\ (\varepsilon v_\parallel^2 + Z_i), \tag{2}$$

where $\varepsilon = E/E_c$ and a, b, c, d are constants to fit (1) to the 2-D numerical results in a region of overlap. We note that although their function F does not scale correctly with $v_\parallel$ ($F \simeq 1 + \text{const}/\varepsilon v_\parallel^2$ is obtained in Ref. 10 and independently in Sec. III of the present work), the procedure gives good results because the Landau resonance falls into the region where f is determined numerically from the 2-D Fokker-Planck code, and only the ADR is situated in the extrapolated region. There, however, f is relatively flat and the scaling with $v_\parallel$ no longer matters. Following the outlined procedure they find that for $\varepsilon \leq 0.1$ and $\omega_{pe}/\Omega_{ce} \leq 2$ the distribution is stable up to $v_\parallel = v_{AD} \simeq 40$. Only in the extreme case of $\varepsilon = 0.1$, $\omega_{pe}/\Omega_{ce} = 2$ and $Z_i = 1$ an unstable mode was found with $v_L = 10$ and $v_{AD} = 42.5$.

The other three quoted papers[9,10,11] are analytic studies based on the plausible model runaway distribution function (1), but in each case with different forms of F and $T_\perp$. Parail and Pogutse[8] use $F \simeq 1 + 1/\varepsilon v_\parallel^2$, but they take $T_\perp$ equal to the thermal bulk temperature, and assume $k_\perp v_\perp/\Omega_{ce} \ll 1$, which is not always true for runaway electrons. With these assumptions they predict instability when $v_{AD} > 3\varepsilon^{-1/2}\ (\Omega_{ce}/\omega_{pe})^{3/2}$. According to this criterion, most of the parameter space found stable in Wiley et al.[12] should be unstable. Liu and Mok[9] use for $T_\perp$ the 2-D analytic result[6]

$T_\perp = (1/\varepsilon)\ \ln \varepsilon v_\parallel$, but for F they take a parallel Maxwellian $\simeq \exp(-v_\parallel^2/v_o^2)$ to approximately account for the loss of runaways from the distribution. The tail cut-off velocity v_o was estimated to lie around 17 v_e. This loss mechanism should enhance the Landau damping and simultaneously decrease the destabilizing effect of the ADR through depression of the runaway tail. None the less instability was found in the region $\omega_{pe}/\Omega_{ce} \geq 0.025/\varepsilon$ for $v_{AD} \leq v_o$, which overlaps the stable region of Wiley et al.[12]. Finally, Gandy et al.[11] use the distribution function of Liu and Mok[9] and consequently obtain some similar results, but also some additional results that appear puzzling. A major question immediately arises from their discussion of Landau damping which they find is larger on the runaway tail than in the bulk between v_e and $v_c = \varepsilon^{-1/2} v_e$. Furthermore, they find in a certain parameter range that the growth rate increases with decreasing electric field. This effect, as the authors later point out, is caused by incorrect normalization of the runaway tail distribution function.

On the basis of the preceding discussion we conclude that modeling of the distribution function, aimed at analyzing stability with respect to the anomalous Doppler resonance, must be done very carefully.

The plan of this paper is as follows. In Sec. II we describe our 2-D Fokker-Planck code and discuss some basic properties of the distribution function. In Sec. III, the results of Sec. II are combined with single-particle dynamics to determine the runaway distribution function in ana-

lytic form. In sec. IV we deal with the instability threshold, and present our conclusions.

II. RUNAWAY DISTRIBUTION FUNCTIONS

We will employ the fast test-electron kinetic model formulated by Kulsrud et al.[13] for simulating runaway distribution functions. The model is described in sufficient detail in Refs. 12 and 13, its characteristic feature being a linear collision operator describing the interaction of fast test electrons with fixed Maxwellian field electrons and ions. While on the one hand the model does not completely account for total electron momentum and energy conservation, the frozen bulk annihilating the excess momentum and energy absorbed from the field, on the other hand the model is adequate for describing fast electrons, and guarantees the existence of a steady state without the necessity of having to further model bulk momentum and bulk energy loss mechanisms. With these stipulations, the electron distribution function f is described by the Fokker-Planck equation

$$\frac{\partial f}{\partial t} = -\text{div}\ \vec{S}, \tag{3}$$

where $\vec{S}$ is the test-electron flux. In spherical coordinates (v, $\mu = v_{\parallel}/v$), we have

$$S_v = \mu\ \varepsilon\ f - \frac{B}{v^3}\left(vf + \frac{\partial f}{\partial v}\right) \tag{4a}$$

$$S_\mu = (1-\mu^2)^{\frac{1}{2}}\left(-\varepsilon f + \frac{A}{2v^2}\frac{\partial f}{\partial \mu}\right). \tag{4b}$$

The equilibrium solution of Eq. (3) with $\varepsilon = 0$ is the Maxwellian

$$f_M = (2\pi)^{-3/2} \exp(-v^2/2). \tag{5}$$

We use the normalized variables

$$t \to t\nu_0,\ v \to v/v_e,\ v_e^2 = kT/m_e,\ (T_e = T_i = T),\ f \to f v_e^3 \tag{6}$$

$$\varepsilon = \frac{E}{E_c},\ E_c = \frac{m_e v_e \nu_0}{e},\ \nu_0 = \frac{4\pi n_e e^4 \ln\Lambda}{m_e^2 v_e^3},$$

and the coefficients A(v) and B(v) are $A = A_e + A_i$, $B = B_e + B_i$, where[13]

$$A_e = \left[\phi(x) - G(x)\right]\Big|_{x = v/\sqrt{2}} \tag{7a}$$

$$A_i = Z_i \left[\phi(x) - G(x)\right]\Big|_{x = (m_i/m_e)^{1/2} v/\sqrt{2}} \tag{7b}$$

$$B_e = v^3 G(x)/ x\sqrt{2}\Big|_{x = v/\sqrt{2}} \tag{8a}$$

$$B_i = v^3 Z_i (m_i/m_e)^{1/2} G(x)/ x\sqrt{2}\Big|_{x = (m_i/m_e)^{1/2} v/\sqrt{2}} \tag{8b}$$

and

$$\phi(x) = \mathrm{erf}(x), \qquad G(x) = \left[\phi(x) - x\,\phi'(x)\right]/ 2x^2. \tag{9}$$

For $v > 1$, we have $A \simeq 1 + Z_i$, $B \simeq 1$.

To integrate Eq. (3) we use the finite-element code TWODEPEP[14]. We directly solve the boundary-value problem for a steady state, $\partial f/\partial t = 0$. A more detailed discussion on the use of the code to solve the steady-state Fokker-Planck equation $\mathrm{div}\vec{S} = 0$ is given in Ref. 15.

The distribution function is generated on a domain (v, μ) with boundary values as depicted in Fig. 1. The component S_μ of the particle flux vanishes at $\mu = \pm 1$ on grounds of symmetry around $v_\perp = 0$. Imposition of the condition $f = \text{const}$ at $v = 0$ is equivalent to including in a time dependent code a source of particles that replenishes the bulk at exactly the same rate at which particles run away. The runaway tail in this problem is thus supported by a steady bulk and the number of particles in the distribution is therefore not conserved. The runaway tails thus formed should be good approximations of tails produced from bulk distributions that are not continuously replenished, as long as the number of particles in the bulk remains much larger than the number of particles in the tail. Finally, at the upper bound of integration $v = v_{max}$ we should impose the flux condition $S_v \simeq \varepsilon\mu f$, but instead we set $f = 0$. This is done out of purely economic reasons to reduce the large number of elements required in the code when the flux boundary condition is used.

In order to scrutinize the runaway distributions thus produced, we first compare in Table I selected values of the runaway production rate Γ (defined as the electron flux through a spherical surface of radius v)

$$\Gamma = 2\pi\, v^2 \int_{-1}^{1} d\mu\, S_v \tag{10}$$

with results obtained in other studies[12,13]. For any particular ε the value of Γ was monitored along the runaway tail, and, as expected, it remained constant except in a narrow region at the upper bound of integration where the imposed condition f = 0 distorts the distribution. A typical 2-D runaway distribution together with flux streamlines [16] is shown in Fig. 2. A different representation is in Fig. 3, where we plot the perpendicular velocity moments of f, the "parallel" distribution function F and the "perpendicular temperature" $T_\perp$,

$$F = 2\pi \int_{0}^{\infty} dv_\perp\, v_\perp\, f = \langle f \rangle,\quad T_\perp = \frac{\langle v_\perp^2 f \rangle}{2F}. \tag{11}$$

We observe a runaway tail forming as expected near $v_\parallel \simeq \varepsilon^{-\frac{1}{2}} = 5$. The sudden drop in F at $v_{\parallel max} = 30$ is a local deformation caused by the boundary condition f = 0. At the critical velocity $v_c = \varepsilon^{-\frac{1}{2}}$, $T_\perp$ starts increasing which signifies the presence of fast particles whose distribution is broadened in the perpendicular direction. The large $T_\perp$ seen on the side of negative $v_\parallel$ is caused by the predominance there of suprathermals pitch-angle-scattered out of the runaway region. In contrast, the bulk is dominated by the thermal particles. The peak in T and the subsequent decline is caused by the diminishing extent of $v_\parallel$ as $v_\perp$ approaches $v_{max} = 35$ (the computation in performed within the circle $v = v_{max}$). If the integration domain were extended we would expect to observe an increasing $T_\perp$.

The presence of a perpendicularly broadened distribution of suprathermals is further witnessed in Figs. 4 and 5. In Fig. 4 we show perpendicular cuts of f at six different positions $v_\parallel$. Although for $|v_\parallel| < v_c$ the population is dominated by thermals having $T_\perp = 1$ (as is apparent from Fig. 3b) the first two cuts in Fig. 4, at $v_\parallel = 2$ and 3, show the presence of a hot tail. The distribution function f is thus everywhere made up of two components, the thermal component dominating in the bulk, and the perpendicularly broadened one dominating outside the bulk. The broadened distribution is obviously near-Maxwellian. Further evidence for the presence of a perpendicularly broadened component is given in Fig. 3, where we plot the perpendicular moments $\tilde{F}_n$ of the deviation from a Maxwellian

$$\tilde{F}_n = \langle v_\perp^n (f - f_M) \rangle , \qquad n = 0, 2, 4. \tag{12}$$

We see that the perpendicular temperature of the perturbation, $\tilde{T} = \tilde{F}_2/2\tilde{F}_o$, is indeed large outside the bulk. In the bulk $\tilde{T}$ is only slightly larger than $T_{bulk} = 1$, because the deviation of f from a Maxwellian is there dominated by an E-induced shift responsible for the bulk current. This part of the perturbation, proportional to $\varepsilon\mu$, becomes negative for negative $v_\parallel$, and its effect is to make the total perturbation negative in the bulk for negative $v_\parallel$. The negative sections appear as interrupted lines in Fig. 5a. The result of Fig. 5b, where we plotted $\tilde{F}_2/2\tilde{F}_0$ and $\tilde{F}_4/4\tilde{F}_2$, serves to further reinforce what we saw in Fig. 4, namely that f is Maxwellian in the perpendicular direction. More specifically, we are referring to the particular property $\tilde{F}_2/2\tilde{F}_0 = \tilde{F}_4/4\tilde{F}_2$ valid for Maxwellians.

III. ANALYTIC SOLUTIONS IN THE RUNAWAY REGION

In the 2-D Fokker-Planck calculations velocity-space is limited to $v \leq 35$ by available memory size. In order to extend the distribution function in the runaway region beyond this range, we make use of the result obtained in Fig. 4, namely that the runaway distribution function f is Maxwellian in the perpendicular direction. We can thus write for $v_{\|} > v_c$

$$f \simeq \frac{F(v_{\|})}{2\pi\, T_{\perp}(v_{\|})} \exp\,(-v_{\perp}^2/2T_{\perp}), \tag{13}$$

where we know from 2-D theory of the runaway tail[5,6] that $T_{\perp}$ scales as

$$T_{\perp} \simeq \frac{(1 + Z_i)}{\varepsilon} \ln\,(v_{\|}\varepsilon^{\frac{1}{2}}) \tag{14}$$

and that

$$F \simeq \Gamma(\varepsilon)/\varepsilon, \tag{15}$$

where Γ is the runaway producton rate[6]

$$\Gamma \simeq 0.35\ \varepsilon^{-3\xi/8} \exp\,[-1/4\varepsilon - (2\xi/\varepsilon)^{\frac{1}{2}}] \tag{16}$$

with $\xi = (1 + Z_i)/2$. The scaling of Γ with ε is confirmed very well for

$Z_i = 1$ by our 2-D calculations (c.f. Fig. 6). However, the functions (14) and (15) are the far-asymptotic (i.e. $v_\parallel \gg v_c$) expressions for $T_\perp$ and F so that they need to be specified in more detail if they are to be of any use in growth rate calculations. Of particular importance is to establish the scaling of F with $v_\parallel$, since the magnitude of Landau damping depends on $dF/dv_\parallel$.

The functions $F(v_\parallel)$ and $T_\perp(v_\parallel)$ are derived in detail in Ref. 17. We outline here the principal steps, based on the fact that in the runaway region an electron is not collision dominated and its average trajectory is given by the test-particle relaxation equations. The relaxation equations are

$$\frac{dv_\parallel}{dt} = \varepsilon - \alpha v_\parallel / v^3; \qquad \alpha = 2 + Z_i \tag{17}$$

$$\frac{1}{2}\frac{dv^2}{dt} = \varepsilon v_\parallel - 1/v, \tag{18}$$

where the electric field acceleration is directed along the positive $v_\parallel$ - axis, and $\varepsilon v_\parallel$ is the rate at which the electron gains energy in the field.

First, as regards the function F, conservation of particles in the E-field-induced flux requires that

$$< f \dot{v}_\parallel > = \text{const} = \Gamma, \tag{19}$$

where $\dot{v}_\parallel$ is given by (17). Upon substitution for f from (13) we get

$$F\left(\varepsilon - \frac{\alpha v_\parallel}{T_\perp} \langle f/v^3 \rangle\right) = \Gamma, \tag{20}$$

where the integral $\langle f/v^3 \rangle$ can be evaluated as

$$\langle f/v^3 \rangle = \frac{1}{v_\parallel} - \left(\frac{\pi}{2T_\perp}\right)^{\frac{1}{2}} e^q \operatorname{erfc}(\sqrt{q}), \tag{21}$$

with $q = v_\parallel^2/2T_\perp$. When $v_\parallel^2 > 2T_\perp$, we find the approximation

$$\langle f/v^3 \rangle \simeq T_\perp/(v_\parallel^3 + 3v_\parallel T_\perp), \tag{22}$$

which yields the simple expression

$$F \simeq \frac{\Gamma}{\varepsilon}\left[1 + \frac{\alpha}{\varepsilon (v_\parallel^2 + 3T_\perp)}\right]. \tag{23}$$

This function, which depends on ion charge through $\alpha = 2 + Z_i$ and $T_\perp$, is in excellent agreement with parallel distribution functions determined numerically from the 2-D Fokker-Planck code. Three examples are presented in Fig. 7. The various cases we have examined cover the interval of ε from $\varepsilon = 0.01$ to $\varepsilon = 0.1$, with $Z_i = 1$, 4 and 9.

Next, to obtain $T_\perp(v_\parallel)$ we eliminate from Eqs. (17) and (18) the time vari-

able and solve for $v_\perp^2/2$ as a function of $v_\parallel$. The starting point is the equation

$$\frac{dy}{dx} + \frac{y}{p} = \frac{\alpha - 1}{p} x \ , \tag{24}$$

where $x \equiv v_\parallel^2$, $y \equiv v_\perp^2$, and

$$p\ (x,y) = \varepsilon x^{\frac{1}{2}}\ (x + y)^{3/2} - \alpha x. \tag{25}$$

For large enough x we can neglect in (25) the term αx, and we write

$$p \simeq \varepsilon x^2\ (1 + y/x)^{3/2} \equiv \varepsilon x^2 U, \tag{26}$$

where in anticipation of the far-asymptotic behavior (14) we assume that $y/x < 1$. The function $U = 1 + y/x$ is then slow compared with y itself, so that to solve Eq. (25) we treat U as a constant factor, and subsequently in the solution thus obtained allow U to again vary. To solve Eq. (24) we go to the new variable $z = 1/x$, whereby Eq. (24) becomes

$$\frac{dy}{dz} - \frac{y}{\varepsilon U} = \frac{1 - \alpha}{z\varepsilon U}, \tag{27}$$

whose solution is

$$y = e^{z/\varepsilon U}\ \{y_o + (\alpha-1)\ [E_1(z/\varepsilon U) - E_1\ (z_o/\varepsilon U)]\}, \tag{28}$$

where E_1 is the exponential integral. The dominant asymptotic contribution in y is

$$y \simeq \frac{\alpha - 1}{\varepsilon U} e^{z/\varepsilon U} E_1 (z/\varepsilon U), \tag{29}$$

which, upon identifying y with $2T_\perp$, gives

$$T_\perp \simeq \frac{1 + Z_i}{2\varepsilon U} \ln (1 + \varepsilon v_\parallel^2 U). \tag{30}$$

If we neglect the weak effect of U in the argument of the logarithm, and write $U \simeq 1 + 3T_\perp/v_\parallel^2$, then

$$T_\perp \simeq (v_\parallel^2/6) [-1 + (1 + 12T_\infty/v_\parallel^2)^{\frac{1}{2}}], \tag{31}$$

where

$$T_\infty = \frac{1 + Z_i}{2\varepsilon} \ln (1 + \varepsilon v_\parallel^2). \tag{32}$$

The expression (31) gives excellent agreement with numerical integrations of the relaxation equations, as well as with $T_\perp$ from the 2-D Fokker-Planck code. Three examples are presented in Fig. 8. We again caution that the results for $T_\perp$ from the 2-D code are not valid near the upper bound of integration where $T_\perp$ decreases because of limitations on velocity-space.

IV. STABILITY WITH RESPECT TO THE ANOMALOUS DOPPLER RESONANCE

Electrostatic plasma waves propagating in an infinite, uniform plasma immersed in a uniform external magnetic field, are described by the dielectric function[18] ε

$$\varepsilon\,(\vec{k},\omega) = 1 + \sum_j \sum_n \frac{\omega_{pj}^2}{k^2} \int d^3v \, \frac{D_{nj} J_n^2\,(k_\perp v_\perp/\Omega_{ej})}{\omega - k_\parallel v_\parallel - n\Omega_{cj} + i\gamma}, \tag{33}$$

where $j = e, i$, and n runs through the cyclotron harmonics $n = 0, \pm 1, \pm 2, \ldots$ Further

$$\omega_{pj}^2 = 4\pi\, n_j\, e_j^2/m_j, \qquad \Omega_{cj} = |e_j B/m_j c|, \tag{34}$$

J_n is the Bessel function, and

$$D_{nj} = \frac{n\,\Omega_{cj}}{v_\perp} \frac{\partial f_j}{\partial v_\perp} + k_\parallel \frac{\partial f_j}{\partial v_\parallel}. \tag{35}$$

For weakly growing waves, $\gamma \ll \omega$, the dispersion relation and the growth rate are respectively[18]

$$\mathrm{Re}\ \varepsilon = 0, \qquad \gamma = -\left.\frac{\mathrm{Im}\ \varepsilon}{\partial(\mathrm{Re}\varepsilon)/\partial\omega}\right|_{\mathrm{Re}\varepsilon = 0}. \tag{36}$$

Provided that $k_\perp^2/k_\parallel^2 \ll m_i/m_e$, we can neglect the ion contribution in (33), and we get

$$\frac{\omega}{\Omega_{ce}}^2 \simeq \frac{k_\parallel^2}{k^2}\frac{Y^2}{1+Y^2}; \qquad Y = \frac{\omega_{pe}}{\Omega_{ce}} \tag{37}$$

and

$$\gamma = \sum_n \sigma \frac{\pi^2 \omega\, \omega_{pe}^2}{k^2 |k_\parallel|} \int_o^\infty dv_\perp\, v_\perp\, J_n^2 \left(\frac{k_\perp v_\perp}{\Omega_{ce}}\right) D_{ne}(v_\perp, v_{\parallel n}), \tag{38}$$

where $v_{\parallel n} = (\omega - n\Omega_{ce})/k_\parallel$ are the positions of the resonances along $v_\parallel$, and[19] $\sigma = (1-\omega^2)/(1+Y^2-\omega^2)$. The contributions of only the n = 0, -1, +1 resonances need be retained in the sum. Conventionally these three resonances are respectively called the Landau, the anomalous Doppler, and the Doppler resonance, and we label their contributions to (38) as γ_L, γ_{AD} and γ_D. Correspondingly, instead of $v_{\parallel 0}$ and $v_{\parallel \mp 1}$ we use the notation v_L, v_{AD} and v_D. It is convenient to work in the normalized variables (6), to which we add the parameter Y specified in (37) and use

$$\omega \to \omega/\Omega_{ce}, \qquad \gamma \to \gamma/\Omega_{ce}, \qquad k \to kv_e/\Omega_{ce}. \tag{39}$$

The growth rate (38) then becomes

$$\gamma = \sum_{n=0,\,\pm 1} \sigma \frac{\pi^2 \omega Y^2}{k^2} \int_o^\infty dv_\perp\, v_\perp J_n^2 (k_\perp v_\perp)\, D_n(v_\perp, v_n), \tag{40}$$

where

$$v_0 = v_L = \frac{\omega}{k_\parallel},\ v_{-1} = v_{AD} = \frac{\omega + 1}{k_\parallel},\ v_1 = v_D = \frac{\omega - 1}{k_\parallel}, \tag{41}$$

and

$$D_n = \frac{\partial f}{\partial v_\parallel} \text{ sign } (k_\parallel) + \frac{n}{v_\perp |k_\parallel|} \frac{\partial f}{\partial v_\perp} \quad . \tag{42}$$

To begin our analysis, we calculated the distribution function f for a few selected values of ε in the range $0.01 \leq \varepsilon \leq 0.1$, of interest to Tokamaks. We then substitute f into (40) and determine γ within a range of v_L and v_{AD} compatible with the dispersion relation and the upper limit of integration. For $Y = \omega_{pe}/\Omega_{ce}$ we took values ranging from 0.2 to 2, which covers most Tokamak operating regimes. In the given parameter space we found the sum (40) negative, in agreement with Ref. 12, but in disagreement with the analyses in Refs. 9 and 11. We point out, at this opportunity, that because of the difference in the definition of thermal velocity, our values of ε correspond to twice that value in Refs. 9, 10, 11, where $v_e^2 = 2kT_e/m_e$.

The reason behind a negative γ in our calculations is the predominance of Landau damping within the given range of parameters, and we also note that the contribution of γ_D is negligible. To give an example, in the particular case of $\varepsilon = 0.04$, $Y = 1$ and $Z_i = 1$, we observed that with the Landau resonance located at $v_L = 8\ v_c$, γ_L exceeded γ_{AD} by an order of magnitude even as v_{AD} attained the extreme position of $v_\parallel$ allowed in the code.

Consequently, to generate instability the anomalous Doppler resonance must lie much further out on the tail than was previously thought. To better appreciate the extent of velocity-space required, it helps to realize that for the waves in question $v_{AD} > 2v_L$, or more exactly from (37)

$$v_{AD}/v_L > 1 + (1 + Y^2)^{\frac{1}{2}}/Y. \tag{43}$$

To establish the growth rate under these conditions it is no longer feasible to calculate f from the Fokker-Planck code, and instead we will use the analytic results of the preceding section. Specifically, we use for f the form (13), where for F and $T_\perp$ we substitute (23) and (32).

First, we evaluate the integrals in (40), which also will help us to gain some insight into the effect of the various parameters on the growth rate. Only two types of integrals appear in (19), namely

$$\int_o^x x\, J_n^2(\alpha x)\, e^{-\rho x^2}\, dx = \frac{1}{2\rho}\, e^{-\frac{\alpha^2}{2\rho}}\, I_n\left(\frac{\alpha^2}{2\rho}\right) \equiv W_n(\alpha, \rho)$$

$$\int_o^x x^3\, J_n^2(\alpha x)\, e^{-\rho x^2}\, dx = -\frac{d}{d\rho} W_n(\alpha, \rho). \tag{44}$$

The rest is straightforward, and for $k_\parallel > 0$ we obtain

$$\gamma_L = \sigma\, \frac{\pi}{2}\, \frac{\omega Y^2}{k^2} \left\{ w_o(q) \left[F' + F\, \frac{T_\perp'}{T_\perp}\, q \left(\frac{I_1}{I_o} - 1 \right) \right] \right\}_{v_\parallel = v_L} \tag{45}$$

and

$$\gamma_{AD} = \frac{\pi}{2}\frac{\omega_Y^2}{k^2}\ \sigma \left\{w_1(q)\left[F' + F\frac{T_\perp}{T_\perp}\left(q\frac{I_o}{I_1} - q - 1\right)\right.\right. \tag{46}$$

$$\left.\left. + \frac{F}{T_\perp k_\parallel}\right]\right\}_{v_\parallel = v_{AD}},$$

where $w_n(q) = \exp(-q)\, I_n(q)$; I_n are the modified Bessel functions of argument q

$$q = k_\perp^2\, T_\perp\,(v_\parallel), \tag{47}$$

and the prime means differentiation with respect to $v_\parallel$.

We begin the discussion of the growth rate by pointing out that at the Landau resonance the dominant term is F', and typically $q \ll 1$, for which $I_o(q) \simeq 1$. At the anomalous Doppler resonance the dominant term is $F/T_\perp k_\parallel$, but q is not necessarily very small and we cannot automatically use the small argument expansion $I_1(q) \simeq q/2$. This then entails that in the expression for γ_{AD} the factor $T_\perp$ does not cancel out from the dominant term $(F/T_\perp k_\parallel)\, w_1(q)$. An increasing $T_\perp$ has therefore a stabilizing influence, an effect which disappears in the usual small-argument expansion treatment of the growth rate (40). Whether a small-argument expansion can be used obviously depends on the width of f in $v_\perp$, of which $T_\perp$ is a measure.

Instability occurs when $\gamma = \gamma_L + \gamma_{AD} > 0$. The normal Doppler contribution can be neglected since F at $v_\parallel = v_D$ is orders of magnitude smaller than F at v_{AD} (i.e. on the runaway tail). The wave variables ω, $k_\parallel$, $k_\perp$ and the plasma parameter $Y^2 = \omega^2_{pe}/\Omega^2_{ce} \simeq n/B^2$ which go into γ must satisfy the dispersion relation (37), from which we can express, for example, $k_\perp^2$ as

$$k_\perp^2 = \frac{k_\parallel^2}{\omega^2}\left(\frac{Y^2}{1+Y^2} - \omega^2\right) = \frac{1}{v_L^2}\left[\frac{Y^2}{1+Y^2} - \frac{v_L^2}{(v_D - v_L)^2}\right], \tag{48}$$

and we can go from ω, $k_\parallel$ to v_L, v_{AD} by means of the transformation

$$\omega = \frac{v_L}{v_{AD} - v_L}, \quad k_\parallel = \frac{1}{v_{AD} - v_L}. \tag{49}$$

The behavior of γ can be discussed on a qualitative basis by collecting the dominant terms

$$\gamma \simeq w_o(q)\, F' \Big|_{v_L} + w_1(q)\, \frac{F}{T_\perp}\, (v_{AD} - v_L) \Big|_{v_{AD}}, \tag{50}$$

where we recall that $q = k_\perp^2 T_\perp$. To begin, it is useful to realize that for a fixed value of v_{AD}, the function γ goes through a local maximum with respect to v_L. This is because Landau damping dominates for small values of v_L near the bulk on the grounds of large F, and then again dominates for large values of v_L [constrained, of course, by (43)] as $w_1(q)$ becomes

very small. More generally, the unstable region $\gamma(v_L, v_{AD}) > 0$ can be obtained on the basis of (50) in the explicit approximate form

$$v_{AD} \geq v_L + \frac{1 + Y^2}{Y^2} \left[\frac{2}{\varepsilon v_L} + \left(\frac{4}{\varepsilon^2 v_L^2} + \frac{v_L^2 Y^2}{1 + Y^2}\right)^{\frac{1}{2}}\right] \equiv \phi(v_L). \tag{51}$$

The function $\phi(v_L)$ has a local minimum with respect to v_L and therefore a necessary condition for instability is that v_{AD} exceed the minimum ϕ.

This behavior is clearly borne out in Fig. 9, showing stability threshold contours $\gamma(v_L, v_{AD}) = 0$, obtained from (45) and (46) with (23) and (31) for several combinations of $\varepsilon = E/E_c$ and $Y = \omega_{pe}/\Omega_{ce}$. The regions of instability are situated, as expected, around a line $v_L = \text{const}$. The lower branch of the stability boundary is due to strong damping, while the upper branch is due to a vanishing anomalous Doppler contribution as $k_\perp \to 0$. In $(\omega, k_\parallel)$-space, the instability regions must again bifurcate on the line $v_\parallel = \omega/k_\parallel = v_{L(bif)}$, as illustrated in Fig. 10. For example, when $\varepsilon = 0.1$ and $Y = 1$, the unstable region will be restricted to the vicinity of the line $\omega \simeq 10\, k_\parallel v_e$, and the region $\omega \leq 0.6\ \Omega_{ce}$, $k_\parallel \leq 0.03\ \Omega_{ce}/v_e$.

The general picture we offer here is that instability due to the anomalous Doppler resonance does not occur unless v_{AD} exceeds a threshold, identified as the minimum with respect to v_L of the function (51). This threshold position of v_{AD} is generally much larger than the threshold

given by Parail and Pogutse[10], $v_{AD} = 3\ v_c\ (\Omega_{ce}/\omega_{pe})^{3/2}$. Also, the unstable regions obtained here are much smaller than what would be expected on the basis of Refs. 9 and 11. As the threshold in v_{AD} is exceeded, a maximum growth rate is then expected around the line $v_L = v_L(bif)$. Away from this line, a low-v_L threshold arises from strong Landau damping, and a high-v_L threshold arises due to a diminishing anomalous Doppler contribution as $k_\perp^2$ decreases.

In conclusion, the basic observation we made here is that even for strong fields ($E/E_c = 0.1$) and high density over magnetic field ratios ($\omega_{pe}/\Omega_{ce} = 1$), the runaway tail must exceed 30 v_e in order to support growing modes. For plasmas having bulk temperatures around 1 keV this translates into tails extending beyond the velocity of light. Most Tokamak plasmas of current interest therefore require a relativistic treatment of the anomalous Doppler instability, along the lines of Refs. 8 and 20, supported by a relativistic 2-D Fokker-Planck code. This generalization will be the subject of a future paper.

ACKNOWLEDGMENTS

This work was supported in part by Hydro-Quebec Project No. 01584-57358713, in part by DOE Contract No. DE-ACOL-78ET-51013, and in part by NSF Grant ECS 85-15032.

REFERENCES

1 H. Dreicer, Phys. Rev. 117, 329 (1960).

2 A.V. Gurevich, Sov. Phys. JETP 12, 904 (1961).

3 M.D. Kruskal and I.B. Bernstein, Princeton Plasma Physics Laboratory Report No. MATT-Q-20 174, 1962 (unpublished). See National Technical Information Service document no. N6314040 (University of Illinois Nucl. Eng. Rep. COO-2218-17). Copies may be ordered from the National Technical Information Service, Springfield, Virginia 22161. The price is $22.95 plus a $3.00 handling fee. All orders must be prepaid.

4 A.N. Lebedev, Sov. Phys. JETP 21, 931 (1965).

5 J.W. Connor and R.J. Hastie, Nucl. Fusion 15, 415 (1975).

6 R. Cohen, Phys. Fluids 19, 239 (1976).

7 H. Knoepfel and D.A. Spong, Nucl. Fusion 19, 785 (1979).

8 K. Molvig, M.S. Tekula and A. Bers, Phys. Rev. Lett. 38, 1404 (1977).

9 C.S. Liu and Y. Mok, Phys. Rev. Lett. 38, 162 (1977).

10 V.V. Parail and O.P. Pogutse, Nucl. Fusion 18, 303 (1978).

11 R.F. Gandy, D.A. Hitchcock, S.M. Mahajan, and R.D. Bengston, Phys. Fluids 26, 2189 (1983).

12 J.C. Wiley, Duk-In Choi, and W. Horton, Phys. Fluids 23, 2193 (1980).

13 R.M. Kulsrud, Y.C. Sun, N.K. Winsor, and H.A. Fallon, Phys. Rev. Lett. 31, 690 (1973).

14 TWODEPEP, IMSL Problem-Solving Software System for Partial Differential Equations (IMSL, Houston, TX, 1983), IMSL No. TDP-0005, Edition 5.

15 M.M. Shoucri, V. Fuchs, K. Hizanidis, and A. Bers, Tokamak de Varennes, Report TVRI 165, 1984 (unpublished).

16 C.F.F. Karney, submitted to Computer Physics Reports.

17 V. Fuchs, R.A. Cairns, C.N. Lashmore-Davies, and M.M. Shoucri, submitted to Phys. Fluids.

18 N.A. Krall and A.W. Trivelpiece, Principles of Plasma Physics (McGraw-Hill, New York, 1973).

19 S.C. Luckhardt, A. Bers, V. Fuchs, and M. Shoucri, Massachusetts Institute of Technology Report No. PFC/JA-86-18, 1986.

20 K. Molvig, M.S. Tekula, and A. Bers, Massachusetts Institute of Technology Report No. PFC/JA-84-1, 1984.

FIGURE CAPTIONS

Fig. 1 Region of integration and boundary conditions for the Fokker-Planck equation (3).

Fig. 2 2-D numerical integration. a) Contourplot of the distribution function f. b) Orientation of the flux $\vec{S}$ and contourplot of the stream function $2\pi\int_{\mu}^{1} d\mu' \, S_v(v,\mu')$.

Fig. 3 2-D numerical integration. Perpendicular-velocity moments of f: the parallel distribution function F and the perpendicular temperature $T_\perp$ as functions of $v_\parallel$.

Fig. 4 2-D numerical integration. Cuts of the distribution funcion f as a function of $v_\perp^2$, taken at six different positions of $v_\parallel$.

Fig. 5 2-D numerical integration. Perpendicular-velocity moments of the deviation $f = f - f_M$, of f from a Maxwellian, as a function of $v_\parallel$. Interrupted lines signify negative values of the functions.

Fig. 6 The runaway production rate Γ (in units $n\nu_o$) as a function of $\varepsilon = eE/mv_e\nu_o$, for $Z_i = 1$. Full line: theory of Refs. 3, 5 and 6 with the pre-exponential factor 0.35 from Ref. 13. Points: present numerical results.

Fig. 7 Comparison of 2-D numerical and analytic [Eq. (23)] runaway distribution functions F.

Fig. 8 Comparison of 2-D numerical and analytic [Eq. 31)] perpendicular temperatures $T_{\perp}$.

Fig. 9 Stability boundaries $\gamma\ (v_L,\ v_{AD}) = 0$ for several combinations of $\varepsilon = E/E_c$ and $Y = \omega_{pe}/\Omega_{ce}$.

Fig. 10 Stability boundary $\gamma = 0$ in $(\omega,\ k_{\parallel})$-space.

RUNAWAY PRODUCTION RATE, $\Gamma = 2\pi v^2 \int_{-1}^{1} d\mu S_v$

Reference	ϵ=0.04 Z_i=1	ϵ=0.06 Z_i=1	ϵ=0.08 Z_i=1	ϵ = 0.1 Z_i = 1	Z_i = 2	Z_i = 3	Z_i = 10
PRESENT	1.92×10^{-6}	5.42×10^{-5}	3.09×10^{-4}	8.2×10^{-4}	5.26×10^{-4}	3.53×10^{-4}	4.42×10^{-5}
Wiley et al.[12]	1.8×10^{-6}	5.3×10^{-5}	3.0×10^{-4}	8.1×10^{-4}	5.4×10^{-4}	3.4×10^{-4}	3.5×10^{-5}
Kulsrud et al[13]	1.914×10^{-6}	5.411×10^{-5}	3.177×10^{-4}	10.4×10^{-4}	5.839×10^{-4}	3.757×10^{-4}	4.49×10^{-5}
Marx and Berger	1.02×10^{-6}	5.3×10^{-5}	3.1×10^{-4}	9.6×10^{-4}	-----	-----	-----

TABLE I

Computed runaway production rates. Comparison of present data with those obtained in Refs. 12 and 13. The results of Marx and Berger are quoted from Ref. 12.

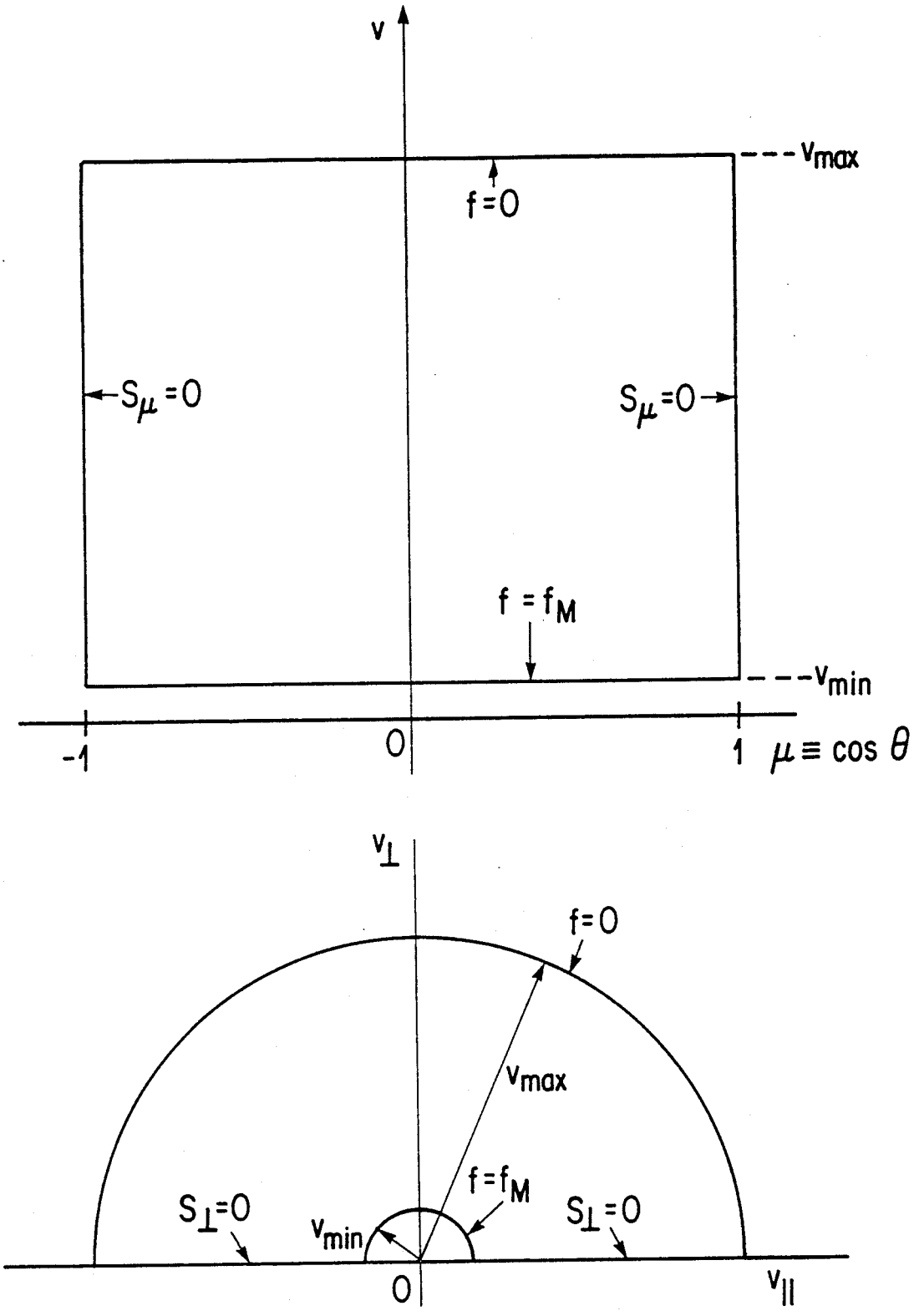
v
v_{max}
f=0
S_μ=0
S_μ=0
$f = f_M$
v_{min}
-1
0
1
$\mu \equiv \cos\theta$
$v_\perp$
f=0
v_{max}
$f = f_M$
$S_\perp$=0
v_{min}
$S_\perp$=0
0
$v_{||}$

FIG. 1

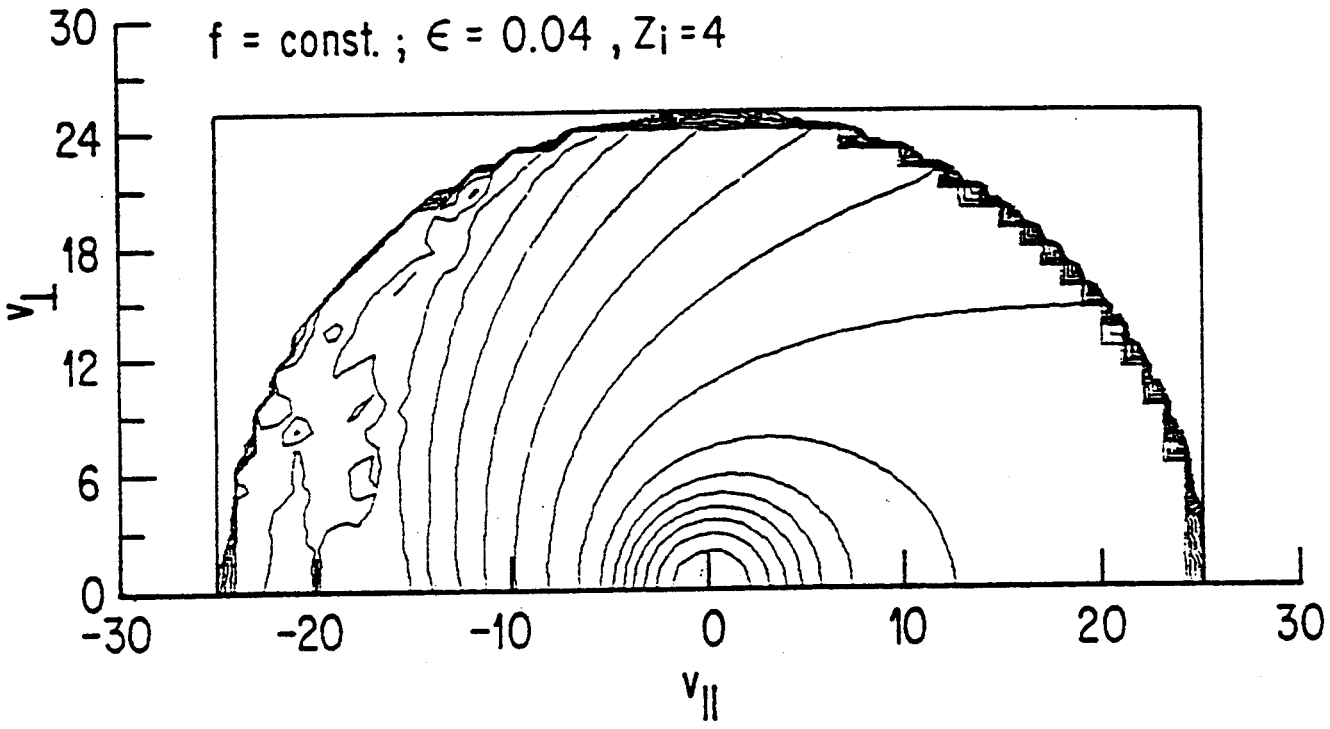

FIG. 2a

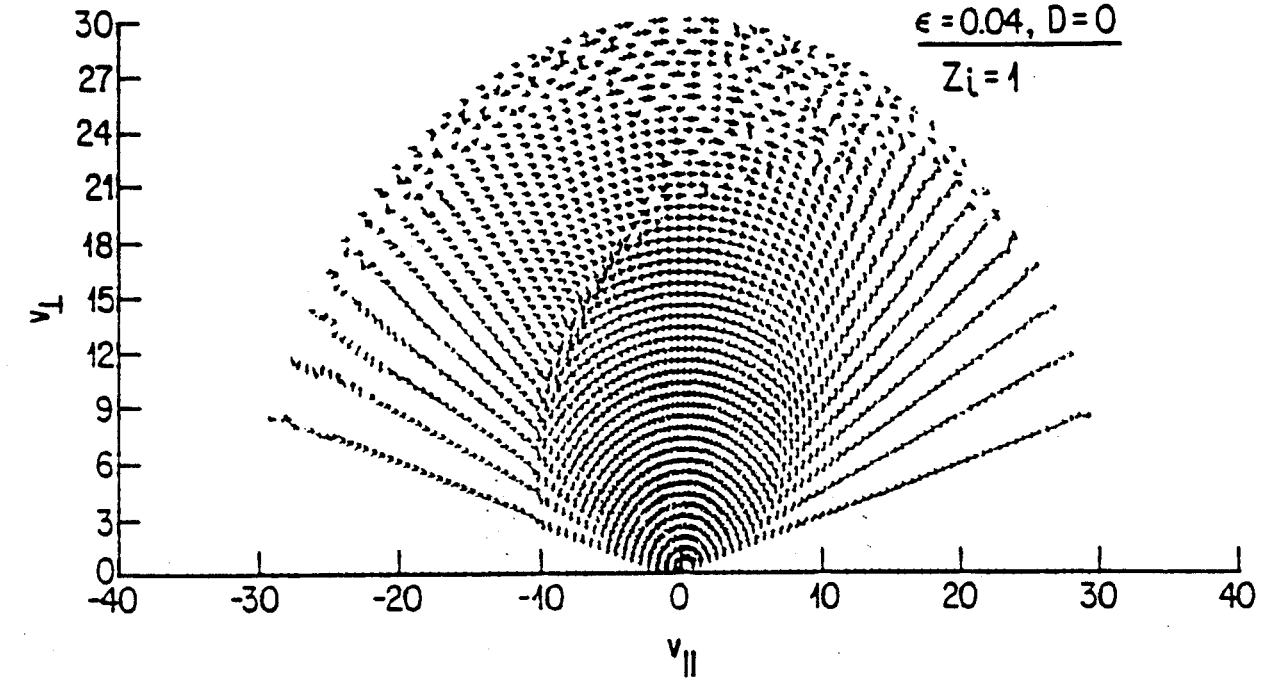
ε = 0.04, D = 0
Zi = 1
30
27
24
21
18
15
12
9
6
3
0
-40
-30
-20
-10
0
10
20
30
40
v⊥
v||

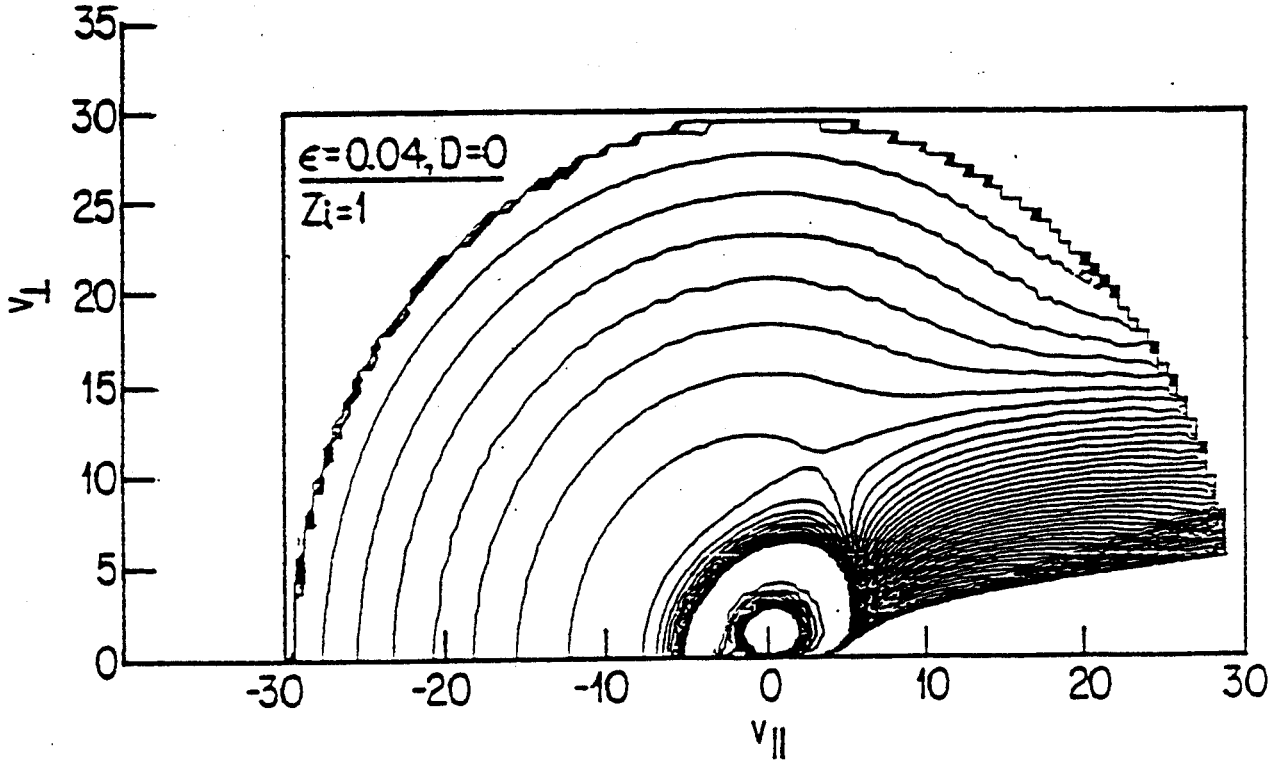
ε = 0.04, D = 0
Zi = 1
35
30
25
20
15
10
5
0
-30
-20
-10
0
10
20
30
v⊥
v||

FIG 2b

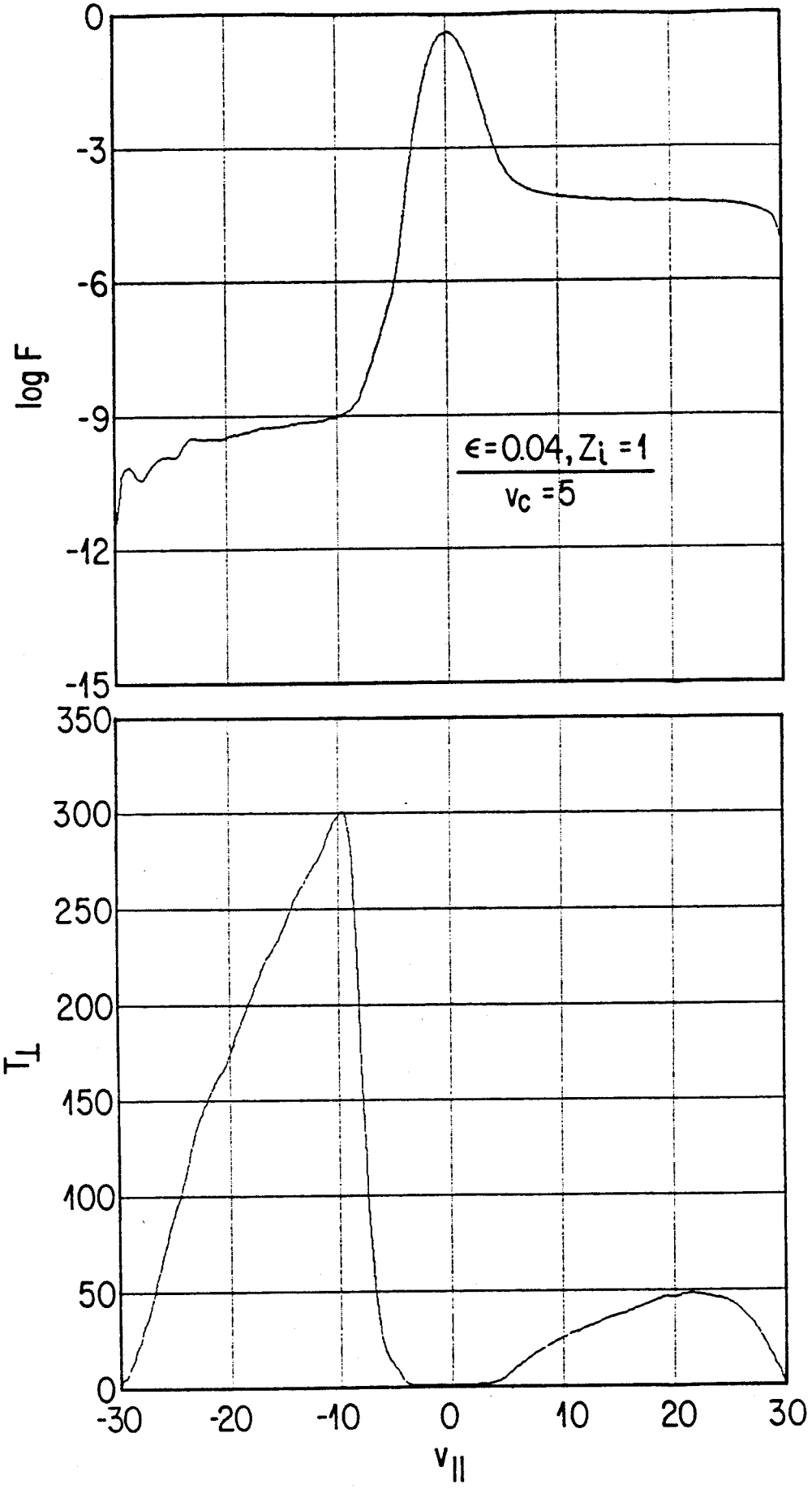
0
-3
-6
-9
-12
-15
log F
ϵ=0.04, Zi =1
vc =5
350
300
250
200
150
100
50
0
T⊥
-30
-20
-10
0
10
20
30
v||

FIG. 3

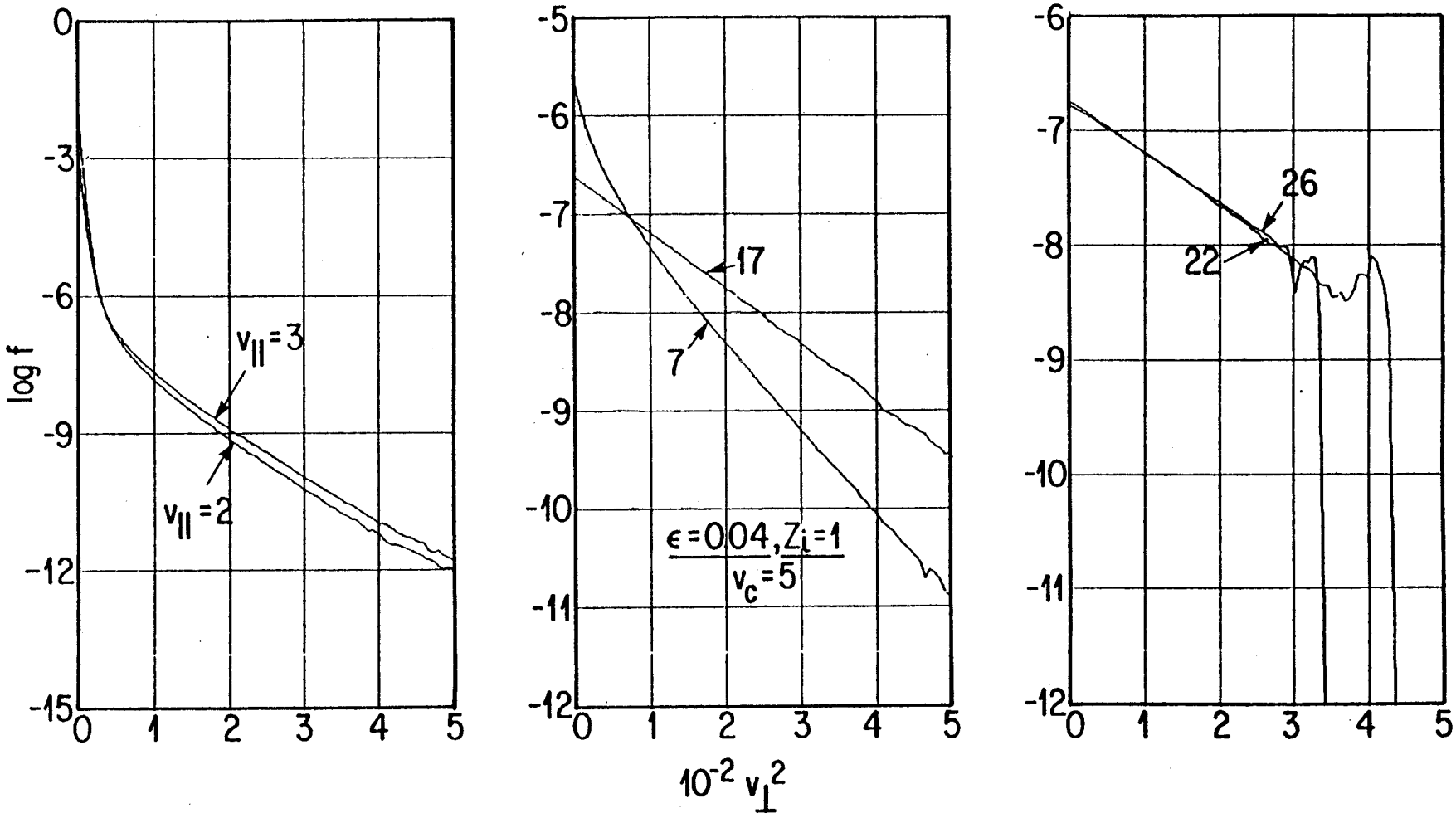
log f
0
-3
-6
-9
-12
-15
0 1 2 3 4 5
$v_{||}=3$
$v_{||}=2$
-5
-6
-7
-8
-9
-10
-11
-12
17
7
$\epsilon=0.04, Z_i=1$
$v_c=5$
$10^{-2}\, v_\perp^2$
-6
-7
-8
-9
-10
-11
-12
26
22

FIG. 4

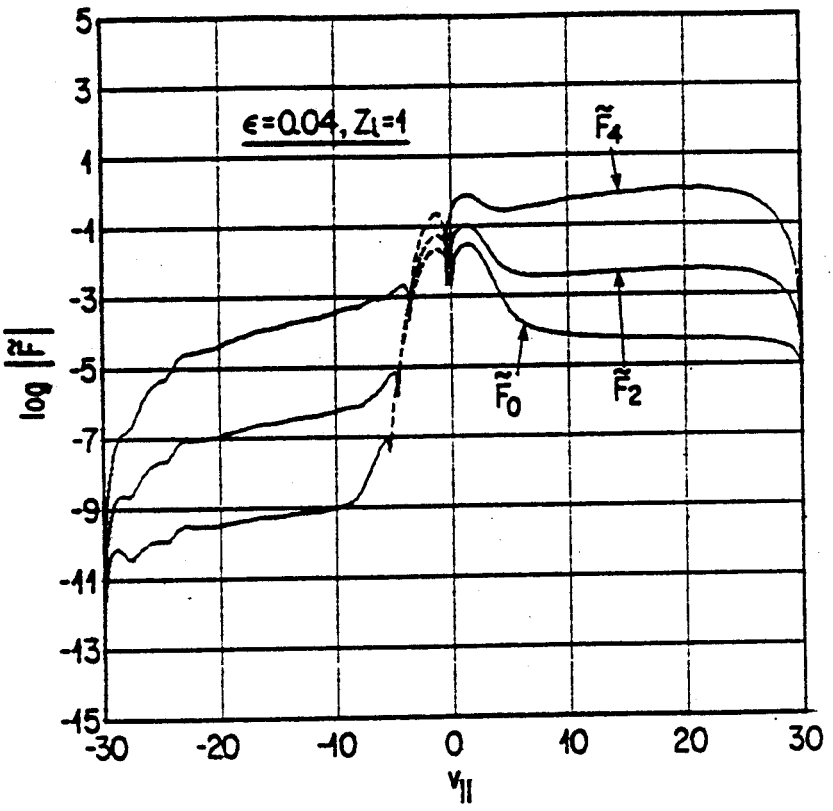

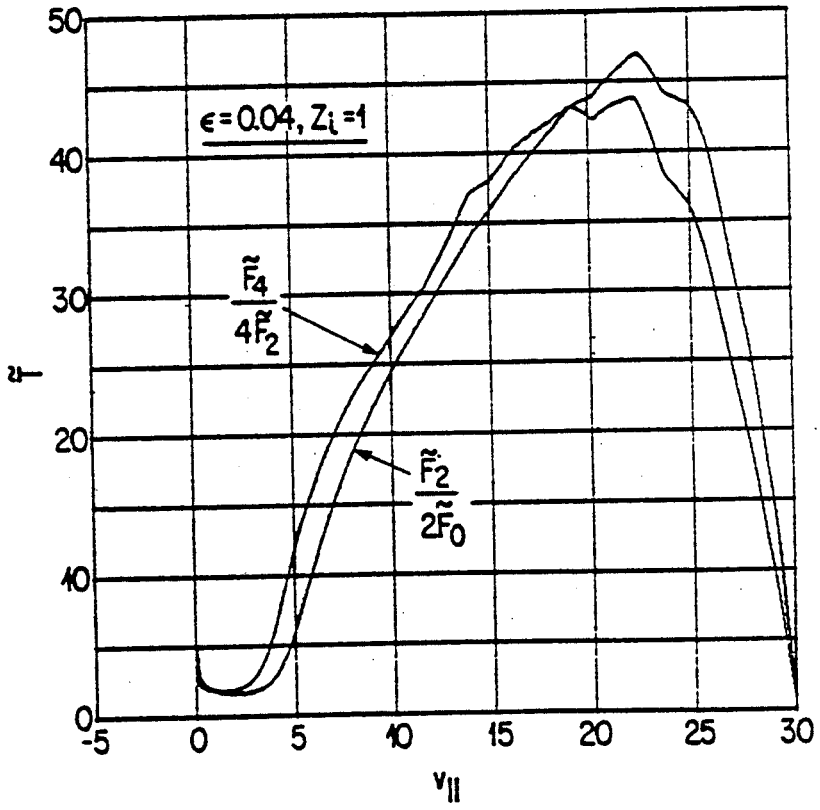

FIG. 5

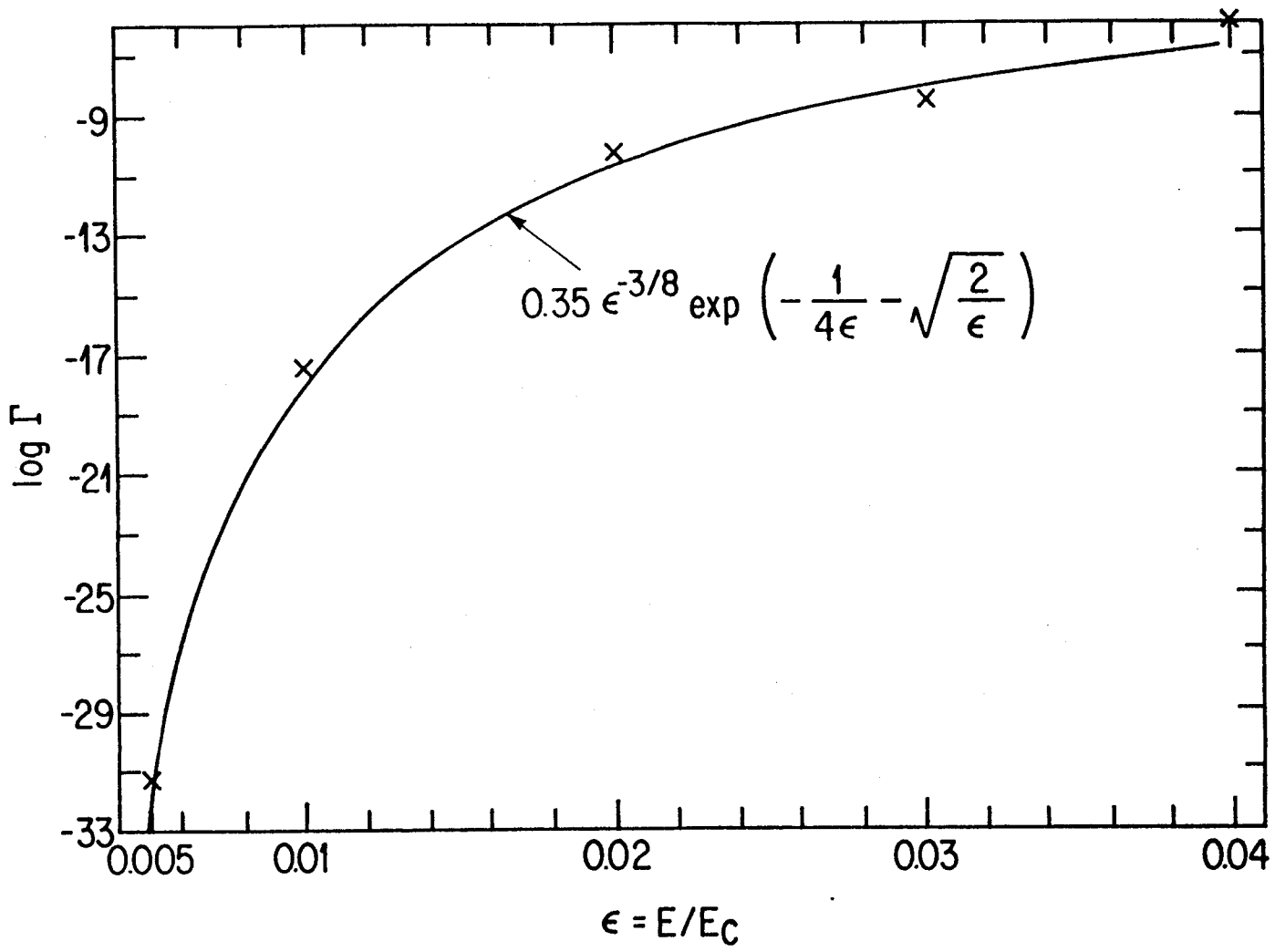
-9
-13
-17
-21
-25
-29
-33
log Γ
0.005
0.01
0.02
0.03
0.04
ε = E/Ec
0.35 ε^-3/8 exp (- 1/4ε - √(2/ε))

FIG. 6

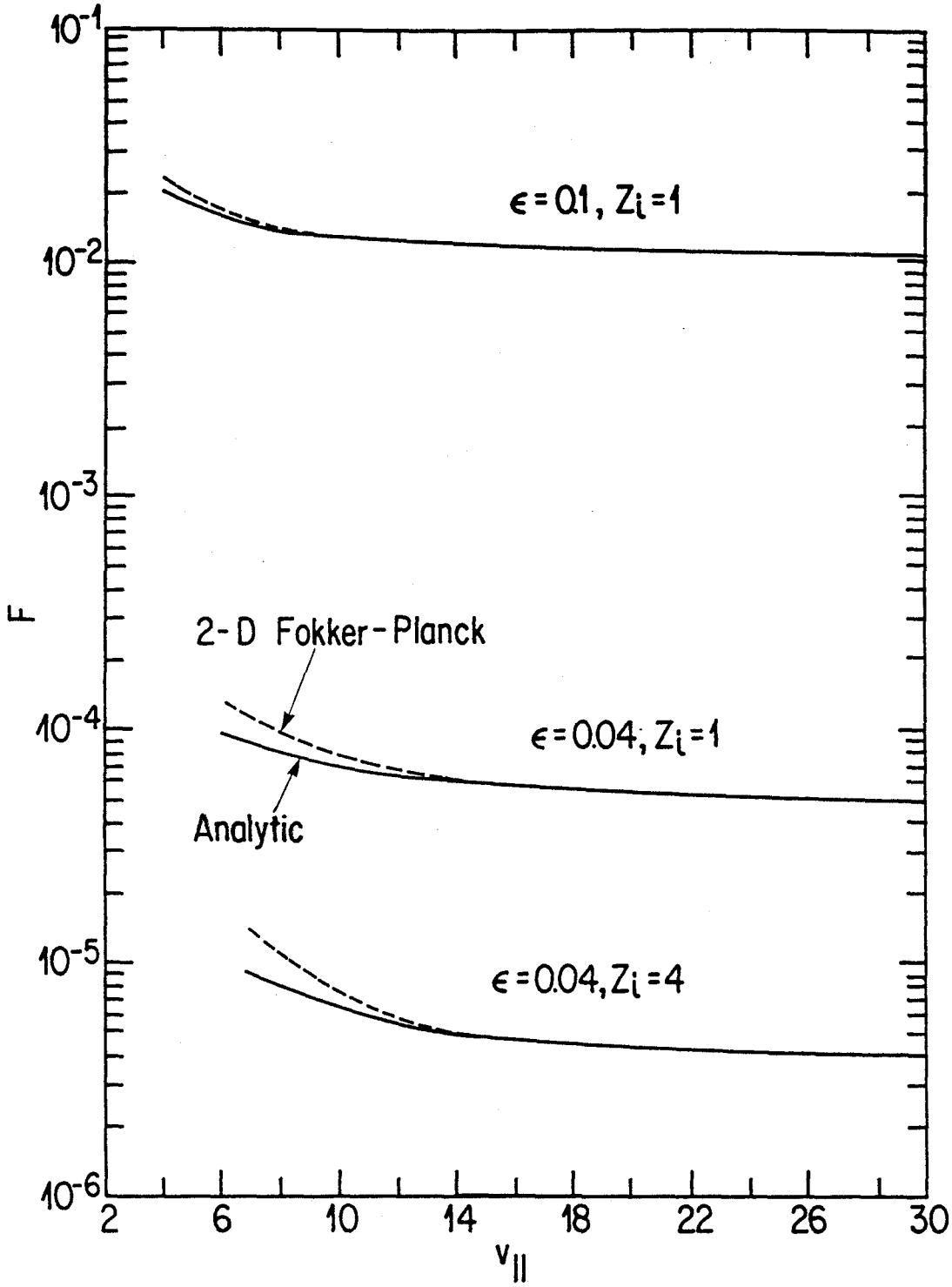
10^{-1}
10^{-2}
10^{-3}
10^{-4}
10^{-5}
10^{-6}
F
$\epsilon = 0.1, Z_i = 1$
2-D Fokker-Planck
$\epsilon = 0.04; Z_i = 1$
Analytic
$\epsilon = 0.04, Z_i = 4$
2
6
10
14
18
22
26
30
$v_{||}$

FIG. 7

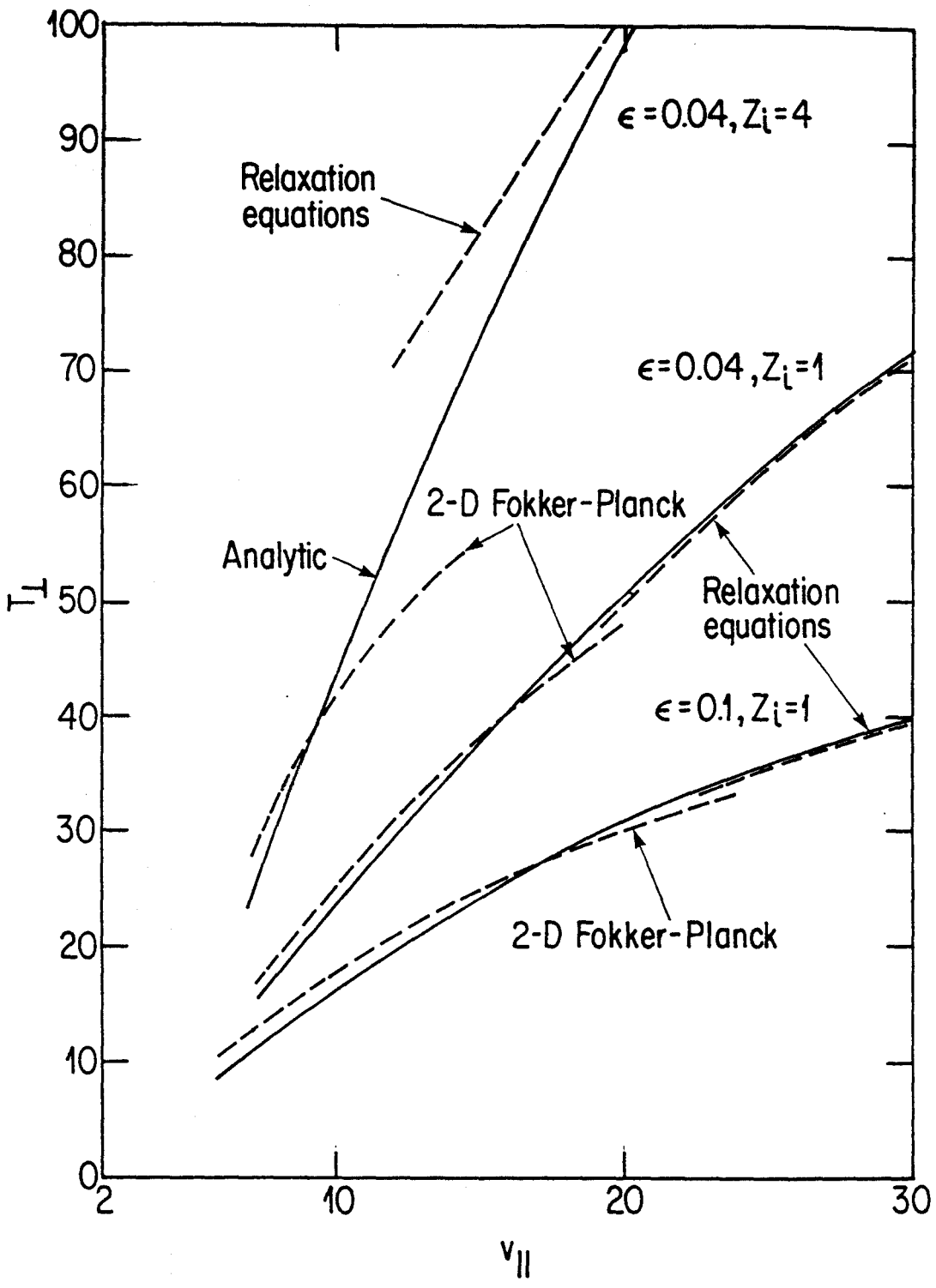
100
90
80
70
60
50
40
30
20
10
0
2
10
20
30
τ_{ii}
v_{ii}
$\epsilon = 0.04, Z_i = 4$
Relaxation equations
$\epsilon = 0.04, Z_i = 1$
2-D Fokker-Planck
Analytic
Relaxation equations
$\epsilon = 0.1, Z_i = 1$
2-D Fokker-Planck

FIG. 8

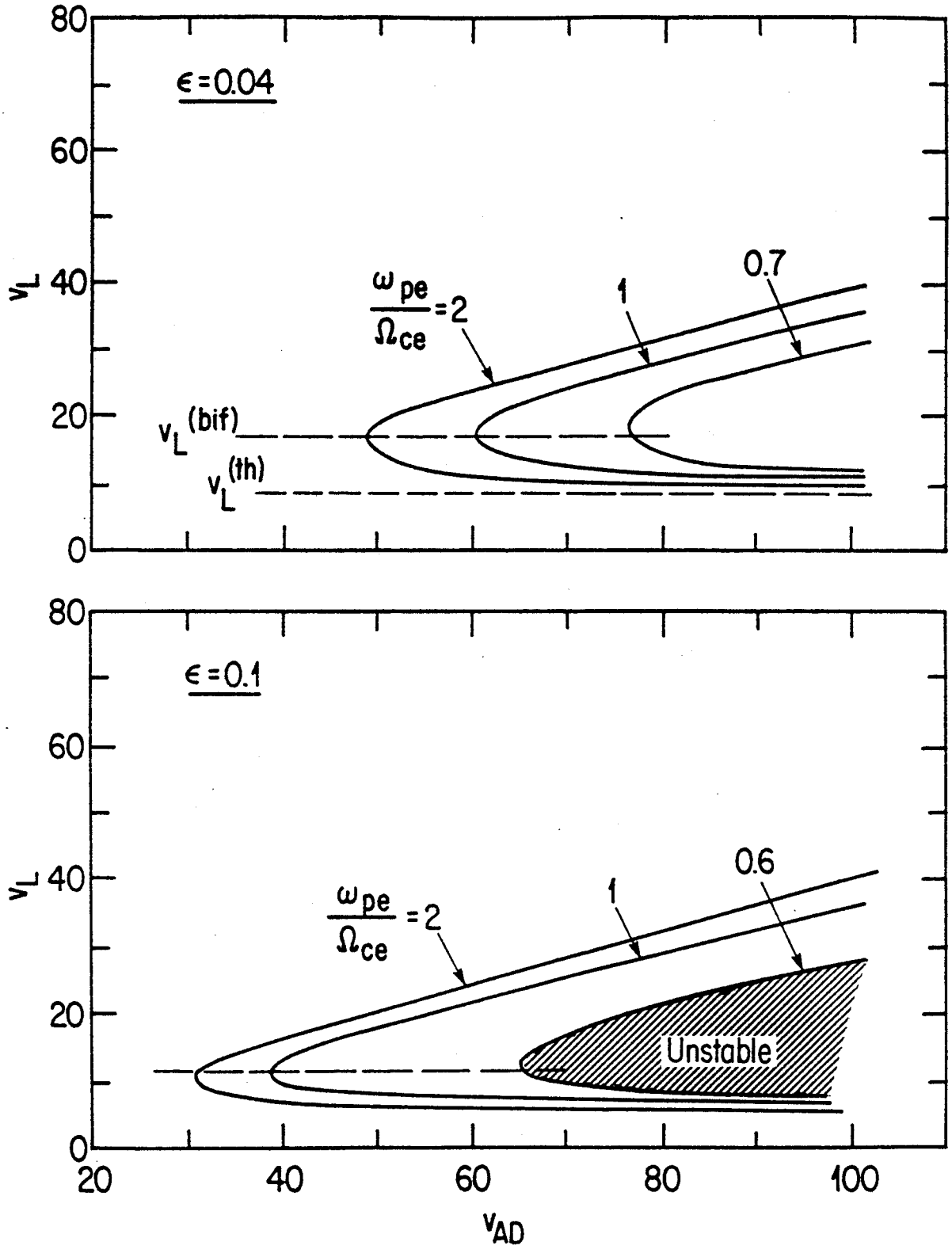
80
60
40
20
0
v_L
$\epsilon = 0.04$
$\frac{\omega_{pe}}{\Omega_{ce}} = 2$
1
0.7
v_L (bif)
v_L (th)
$\epsilon = 0.1$
0.6
Unstable
20
40
60
80
100
v_{AD}

FIG. 9

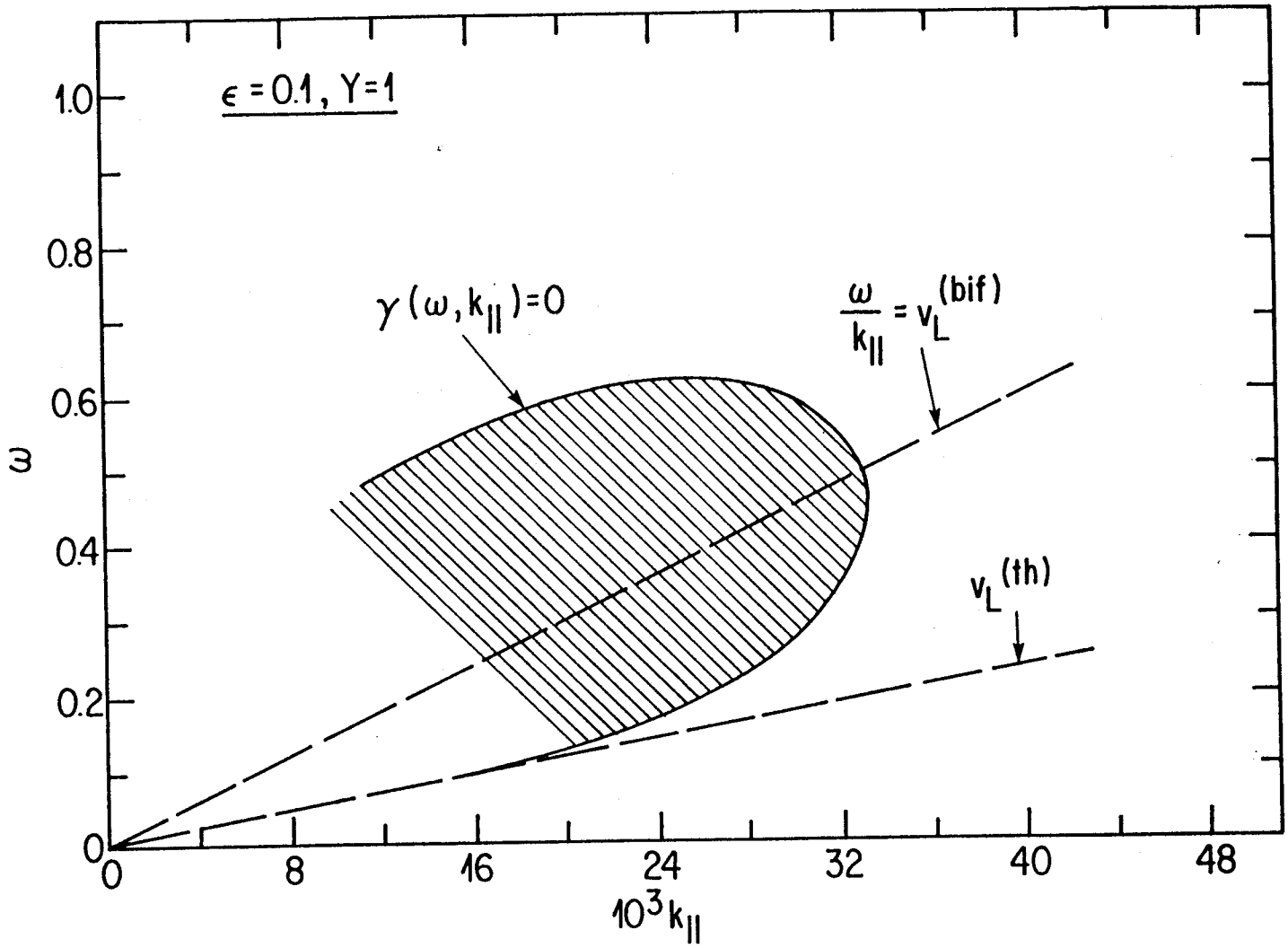

FIG. 10